Electronic Supplementary Material (ESI) for ChemComm.
This journal is © The Royal Society of Chemistry 2018

Supporting Information:

Defect- and phase-engineering in Mn-mediated MoS_2 nanosheets for ultrahigh electrochemical sensing of heavy metal ions: Chemical interaction-driven *in situ* catalytic redox

Wen-Yi Zhou,[‡a,b] Shan-Shan Li,[‡a,b] Xiang-Yu Xiao,[a,b] Shi-Hua Chen,[a,b] Jin-Huai Liu,[a,b] and Xing-Jiu Huang*[a,b]

[a]Key Laboratory of Environmental Optics and Technology and Institute of Intelligent Machines, Chinese Academy of Sciences, Hefei 230031, P.R. China

[b]Department of Chemistry, University of Science and Technology of China, Hefei 230026, P.R. China

[‡]These two authors contributed equally to this work.

*Correspondence should be addressed to X.J.H. (email: xingjiuhuang@iim.ac.cn)

Tel.: +86-551-65591142; fax: +86-551-65592420.

1. Experimental Section

1.1 Pure MoS_2 and Transition Metal-Mediated MoS_2 Preparation

The pure and transition metal-mediated MoS_2 (Mn, Fe, Co, Ni, and Cu) were prepared via a method modified from the literature.[1, 2] Here, 1.164 g $(NH_4)_6Mo_7O_{24}\cdot 4H_2O$, 2.284 g thiourea, and 0.6 mmol transition metal ions ($MnCl_2\cdot 4H_2O$, $FeCl_2\cdot 4H_2O$, $CoCl_2\cdot 6H_2O$, $NiCl_2\cdot 6H_2O$, and $CuCl_2\cdot 2H_2O$) were dissolved in 40 mL deionized (DI) water. The mixture was magnetically stirred for 1 h to obtain a homogeneous solution. Then, the solution was transferred to a 50 mL Teflon-lined autoclave and maintained at 200 °C for 20 h. After cooling to room-temperature, the reaction product was washed with ethanol and DI water and collected via centrifugation. The black product was dried via vacuum freeze-drying technology. To optimize the amount of Mn, 0.4 and 0.8 mmol $MnCl_2\cdot 4H_2O$ were added to prepare the Mn-MoS_2. Pure MoS_2 was prepared similarly without adding transition metal ions.

1.2 Characterization

The morphology and atomic arrangement were characterized by high-angle annular dark-field scanning transmission electron microscopy (HAADF-STEM, Ac-STEM, JEOL ARM-200F), high-resolution transmission electron microscopy (HRTEM) (JEM-2010, JEOL Co.), and scanning electron microscope (FESEM, Quanta 200 FEG, FEI Company, U.S.A.). X-ray diffraction (XRD) patterns were recorded on a Philips X'Pert Pro X-ray diffractometer with Cu Kα radiation (1.5418 Å). The data was analyzed with X'Pert HighScore software.[3] X-ray absorption fine structure (XAFS)

measurements were conducted with the BL14W1 beamline of the Shanghai Synchrotron Radiation Facility (SSRF). The X-ray photoelectron spectroscopy (XPS) measurements were performed on a Thermo ESCALAB 250 spectrometer with an Al Ka X-ray source (1486.6 eV, 150 W) and a constant analyzer. The binding energy of the C1s of contaminated carbon set at 284.8 eV. The XPSPEAK41 procedure analyzed and fit the data. Electron spin resonance (ESR) analyzed the electronic state of transition metal- mediated MoS_2 by JES-FA 200 Spectrometer (JEOL) X-Band. Raman measurements used a Lab RAM HR800 confocal microscope Raman system (Horiba Jobin Yvon). The doping amount was determined by inductively coupled plasma mass spectrometry (VG Elemental PlasmaQuad 3).

1.3 MoS_2 Electrode Fabrication

A traditional drop-coated method was used for electrode modification. Simply, 1 mg of pure or Mn-MoS_2 samples were dispersed in 5 mL of water to form a suspension. Then, 7 μL of the suspension was pipetted onto the surface of a polished glassy carbon electrode (GCE). The solvent was evaporated under room temperature to obtain MoS_2-modified GCE.

1.4 Electrochemical Measurements

All electrochemical tests used a CHI660D computer-controlled potentiostat (Chenhua Instruments Co., Shanghai, China) including a conventional three-electrode system with a modified or bare glassy carbon electrode (GCE, 3 mm diameter) as the

working electrode; Ag/AgCl served as the reference electrode, and a Pt wire was the counter electrode. Square wave anodic stripping voltammetry (SWASV) was used for Pb(II) detection under optimal experimental conditions. A deposition potential of –1.0 V was applied for 120 s to the working electrode with stirring. The SWASV responses were recorded between –1.0 and 0 V with step potential of 4 mV, an amplitude of 25 mV, and a frequency of 15 Hz in HAc-NaAc solution (0.1 M, pH=5.0). A desorption potential of 0.8 V for 120 s removed the residual metal under stirring.

Electrochemical impedance spectroscopy (EIS) was measured at an AC voltage amplitude of 5 mV from 10^5 to 1 Hz in a solution consisting of 5 mM $K_3Fe(CN)_6$ and 0.1 M KCl. Mott-Schottky plots were measured in 0.25 M Na_2S/Na_2SO_3 solution at the fixed frequency of 1000 Hz in the applied voltage range of –1.3 to –0.9 V.

1.5 Adsorption Measurements

Adsorption experiments used a batch technique. The 10 mg of MoS_2 samples and 10 mL of 0.1 mM Pb(II) aqueous solution were combined in a vial at room temperature. The vial was then continuously stirred for 12 h. Next, the adsorbents were separated via high speed centrifugation, and dried via vacuum freeze-drying for further XPS analysis. The pH was controlled at 5.0 by HAc-NaAc (0.1 M) solution.

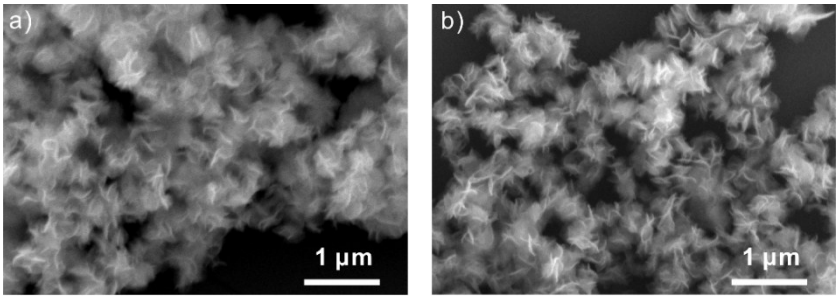

Fig. 1 SEM images of (a) pure MoS_2 and (b) Mn-MoS_2.

The influence of electrochemical experiment parameters, such as supporting electrolytes, deposition potential, deposition time, pH values were investigated. Here, the Mn-MoS_2 modified electrode was chosen to study the optimum experiment conditions. Fig. S2a shows the square wave anodic stripping voltammetry plots toward 0.5 μM Pb(II) by changing the supporting electrolytes (pH = 5.0): NaAc-HAc buffer solution, phosphate buffer solution (0.1 M), and $NH_3 \cdot H_2O$-NH_4Cl solution (0.1 M). The NaAc-HAc buffer was applied in following measurements due to the high signal intensity. The shift of striping signal peak may be ascribed to the influence from different buffer solutions.

Fig. S2b shows the pH value effect on the electrochemical performance toward 0.5 μM Pb(II). The peak current of Pb(II) increases as the pH value changing from 3.0 to 5.0. However, the peak current decreases as the pH value increases further. Therefore, the pH value of 5.0 was determined.

Fig. S2c shows the peak current toward 0.5 μM Pb(II) at a deposition potential range from −0.7 to −1.4 V in NaAc-HAc buffer solution. The peak current increases obviously as the potential shifted from −0.7 to 1.0 V, which is due to the increased

amount of Hg (II) under a negative deposition potential. The peak current reaches the maximum at −1.0 V. The peak current decreases when the potential is beyond −1.0 V, which is because of the interference of hydrogen evolution reaction. The optimum deposition potential was determined as −1.0 V.

Fig. S2d shows the influence of deposition time (30, 60, 90, 120, 150, and 180 s) on electrochemical performance of the Mn-MoS_2 modified electrode toward 0.5 μM Pb(II). With the consideration of efficiency, a deposition time of 120 s was selected for following measurements.

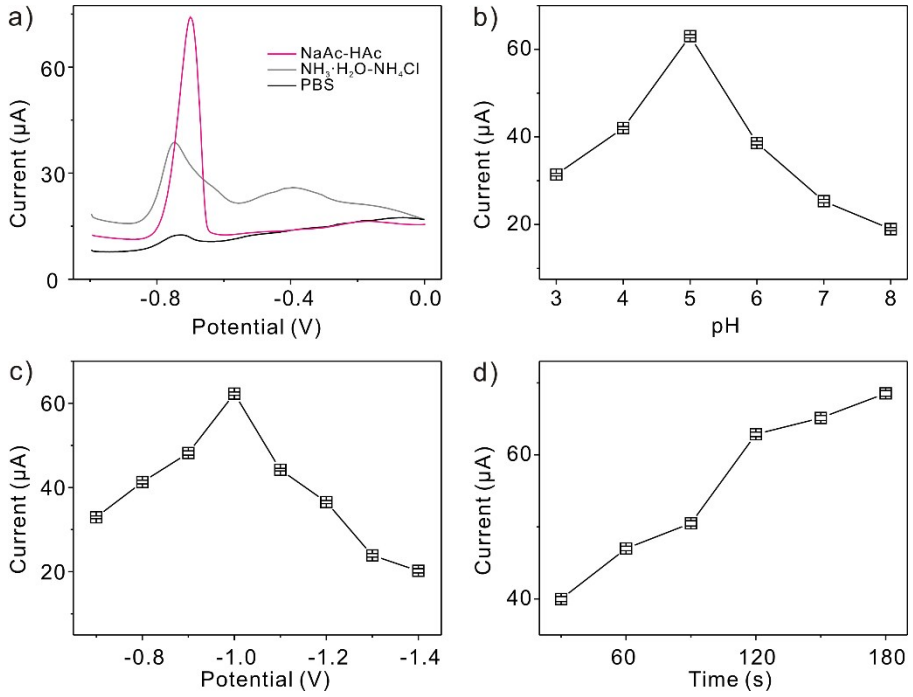

Fig. S2 Optimum experimental conditions. Influence of (a) supporting electrolytes, (b) pH, (c) deposition potential, and (d) deposition time values on the voltammetric response of the Mn-MoS_2 modified GCE. Data were collected from the SWASV response of 0.5 μM Pb(II) on Mn-MoS_2 modified electrode. The error bars represent the standard deviations of five independent measurements of the same sample.

The influence of doping amount (ranging from 0.74 wt.% to 1.21 wt.%, by ICP-MS) of Mn was also investigated (Fig. S3). The amount of 0.92 wt.% in Mn-MoS_2 shows the best electrochemical-sensing performance. The XPS and XRD characterizations are shown in Fig. S4, 5, and 6. New diffraction peaks emerge at 18° and 32° when the Mn doping reaches 1.21 wt.%. The new structure occupies the active sites on Mn-MoS_2, [2] and this might explain the decreased response current. Therefore, the doping amount of 0.92 wt.% in Mn-MoS_2 was selected as the optimum sensing material.

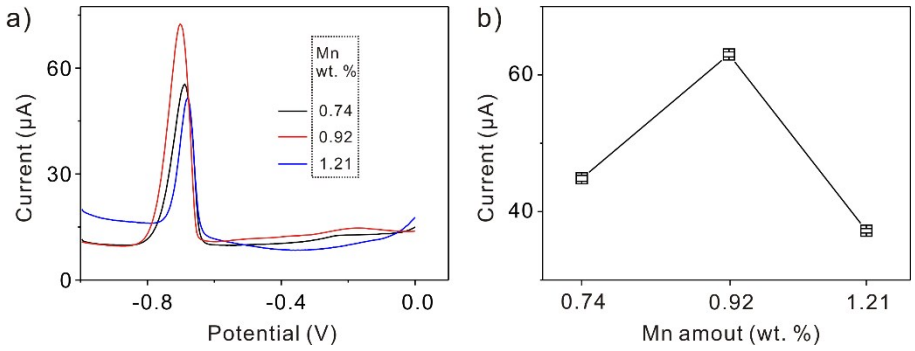

Fig. S3 The influence of doping amount (ranging from 0.74 wt. % to 1.21 wt. %) of Mn. (a) SWASV response of 0.5 μM Pb(II). (b) Corresponding peak current. Error bars correspond to standard errors measured from five independent measurements. The error bars represent the standard deviations of five independent measurements of the same sample.

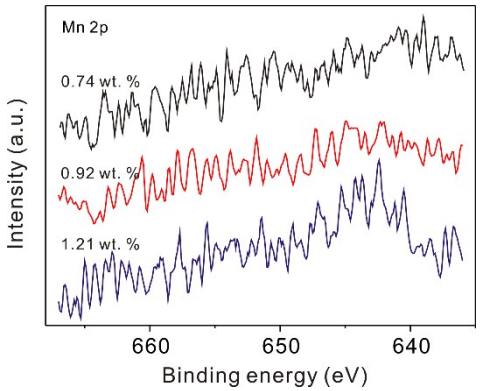

Fig. S4 XPS spectra of three kinds of Mn-MoS_2 in Mn 2p region.

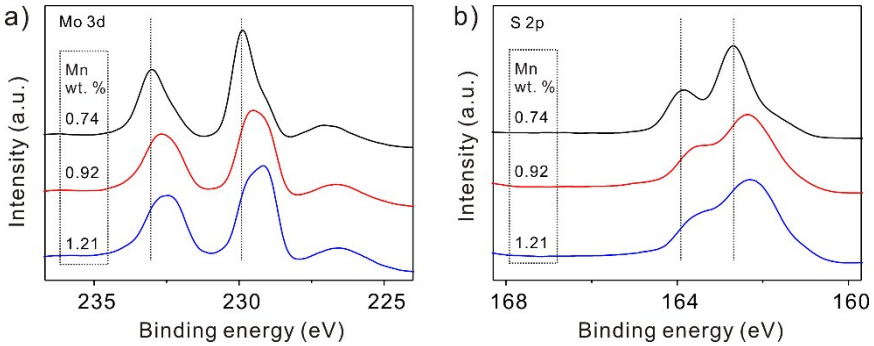

Fig. S5 XPS spectra three kinds of Mn-MoS_2 in (a) Mo 3d and (b) S 2p regions.

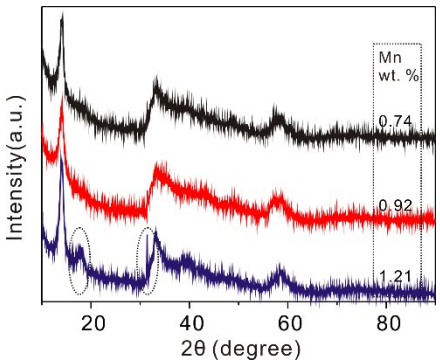

Fig. S6 XRD patterns of three kinds of Mn-MoS_2.

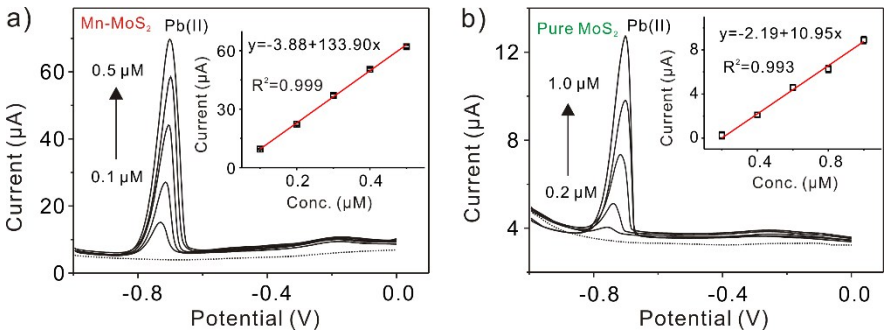

Fig. S7 Typical SWASV responses and corresponding linear calibration plots (insets) of (a) pure MoS_2 and (b) Mn-MoS_2-modified GCE toward Pb(II).

In the pure MoS_2 nanosheets, the Raman spectra (Fig. S8b) display characteristic peaks of 2H-phase.[4] In contrast, Mn-MoS_2 has additional peaks at 219 and 336 cm^{-1}, which is attributed to the 1T-MoS_2 phase. This suggests the existence of a 1T-phase embedded in the 2H-MoS_2. Fig.s 3d and e show the Mo 3d and S 2p XPS spectra. The peaks at 230.1 and 233.2 eV correspond to binding energies of Mo 3d5/2 and 3d3/2 electrons in the 2H-phase, respectively. These are shifted to lower energy by 0.3 eV (Fig. S8c) after the 1T-phase was introduced. This was also observed in a previous report.[1] The new peak at the lower binding energy position along with the initial peak of 2H-phase are revealed by the deconvolution of Mo XPS peak, which suggests the existence of the 1T-phase after Mn-mediating. This is accompanied by clear evidence of Mn−S bonding.[5] Similarly, the 1T-phase is also clearly seen in S 2p spectra of Mn-MoS_2 (Fig. S8d). These results confirm the successful Mn-mediating and subsequent introduction of the 1T-phase into the 2H-phase.

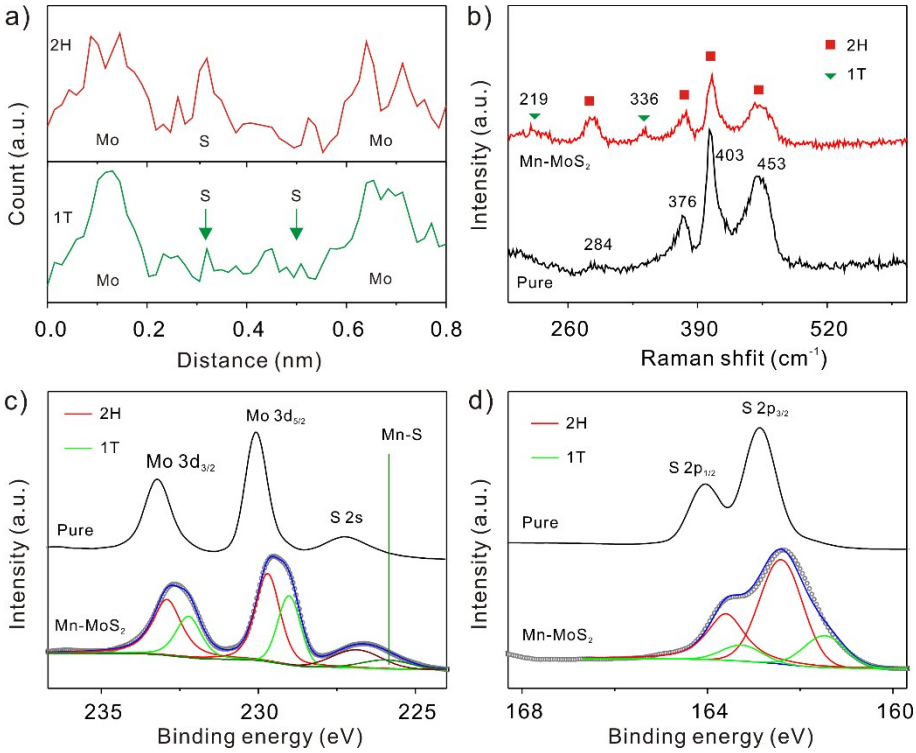

Fig. S8 (a) The intensity profiles of 2H and 1T structures along the lines indicated in Fig. a. (b) Raman spectra, (c) XPS spectra in Mo 3d, and (d) S 2p regions of pure and Mn-MoS_2.

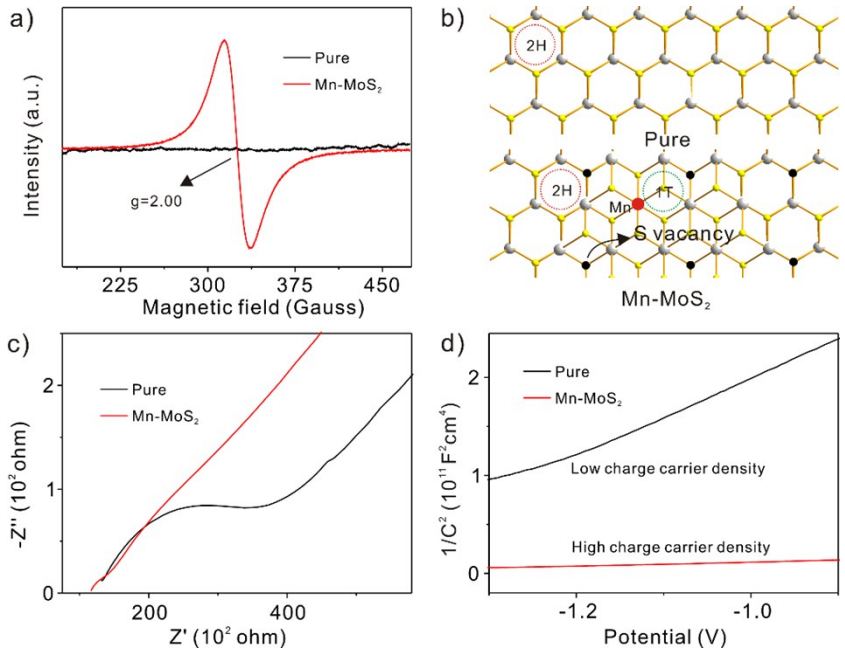

Fig. S9 (a) ESR spectra, (b) structural models (obtained with the help of Diamond

program), (c) EIS, and (d) Mott−Schottky plots of pure and Mn-MoS_2.

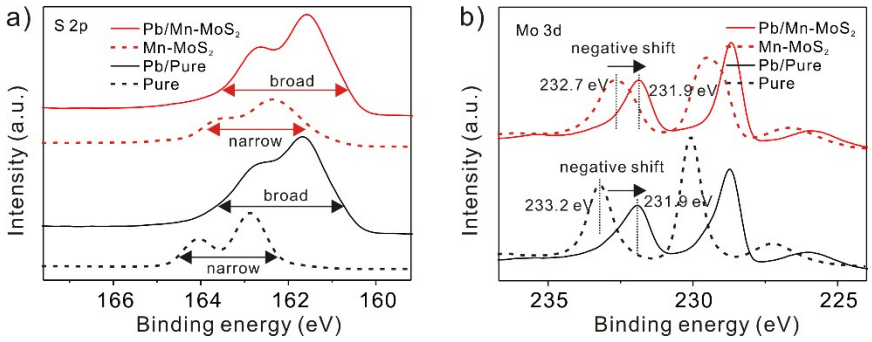

Fig. S10 (a) S 2p and (b) Mo 3d regions of Pb/Mn-MoS_2 and Pb/pure versus pure and Mn-MoS_2.

The sensitivity of different transition metal elements (Fe, Co, Ni, and Cu)-mediated MoS_2 was investigated due to the successful enhancement of electrochemical sensitivity via Mn-MoS_2. The morphologies and XRD patterns of Fe, Co, Ni, and Cu-MoS_2 were similar with that of Mn-MoS_2 (Figures S11 and S12). The XPS spectra show Fe, Co, Ni, and Cu element (Figure S13). The binding energy shift of Mo 3d and S 2p in different elements-mediated MoS_2 can be attributed to the different electronic densities of the dopants. The 2H and 1T states are seen in the XPS data. Figure S14 shows the ESR signals at g=2.00 of the transition metal element-mediated MoS_2 indicating the existence of V_S.

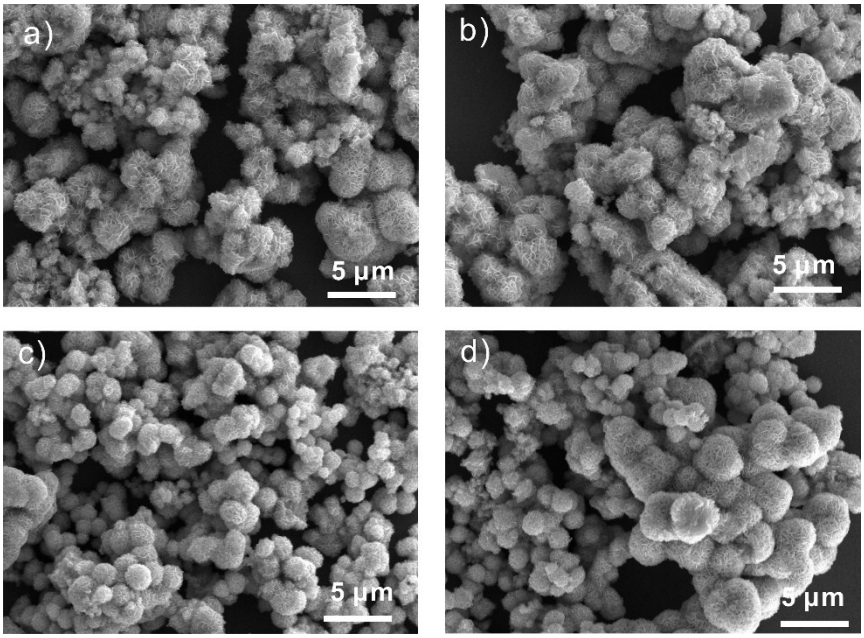

Fig. S11 SEM images of (a) Fe-MoS_2, (b) Co-MoS_2, (c) Ni-MoS_2, and (d) Cu-MoS_2.

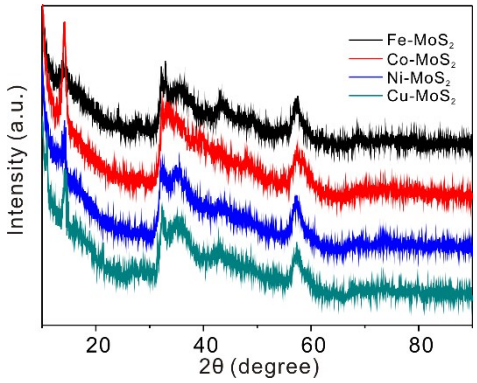

Fig. S12. XRD patterns of Fe-MoS_2, Co-MoS_2, Ni-MoS_2, and Cu-MoS_2.

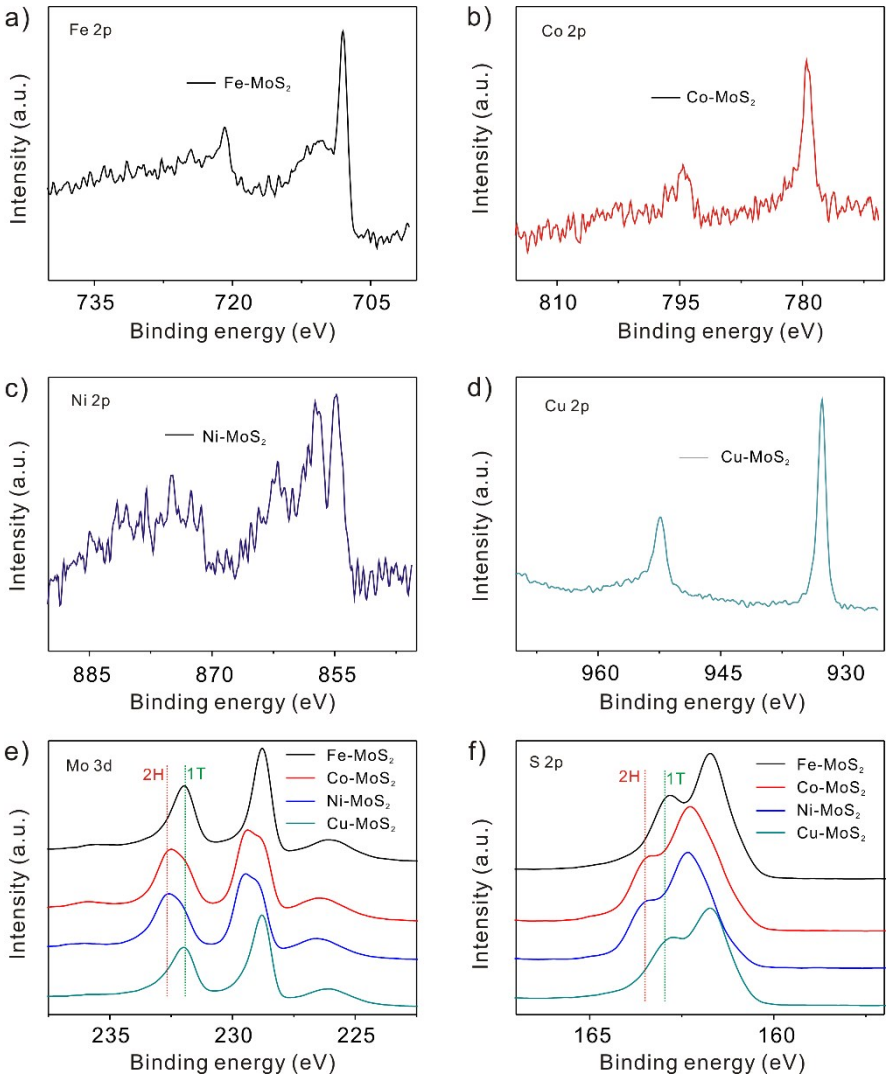

Fig. S13 XPS spectra in (a) Fe 2p region of Fe-MoS_2, (b) Co 2p region of Co-MoS_2, (c) Ni 2p region of Ni-MoS_2, and (d) Cu 2p region of Cu-MoS_2. XPS spectra in (e) Mo 3d region and (f) S 2p region of the transition metal element (Fe, Co, Ni, and Cu) doped MoS_2.

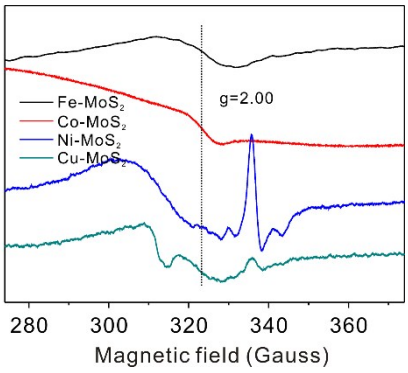

Fig. S14 ESR signals of Fe-MoS_2, Co-MoS_2, Ni-MoS_2, and Cu-MoS_2.

Fig. S15 compares the electrochemical sensitivity of transition metal element-mediated MoS_2. The corresponding stripping signals are shown in Fig. S16. The Fe, Co, Ni, and Cu-MoS_2 have sensitivities of 61.37, 54.08, 38.49, and 21.72 μA μM^{-1}, respectively, which are lower than Mn-MoS_2. The Fe-, Co-, Ni-, and Cu-MoS_2 could be used for hydrogen evolution. The hydrogen evolution result shown in Fig S15b was consistent with the literature.[2] The H_2 that forms during the detection might have an adverse effect.[6] Therefore, the reason for the lower sensitivity of Fe, Co, Ni, and Cu-MoS_2 might be their hydrogen evolution capability.

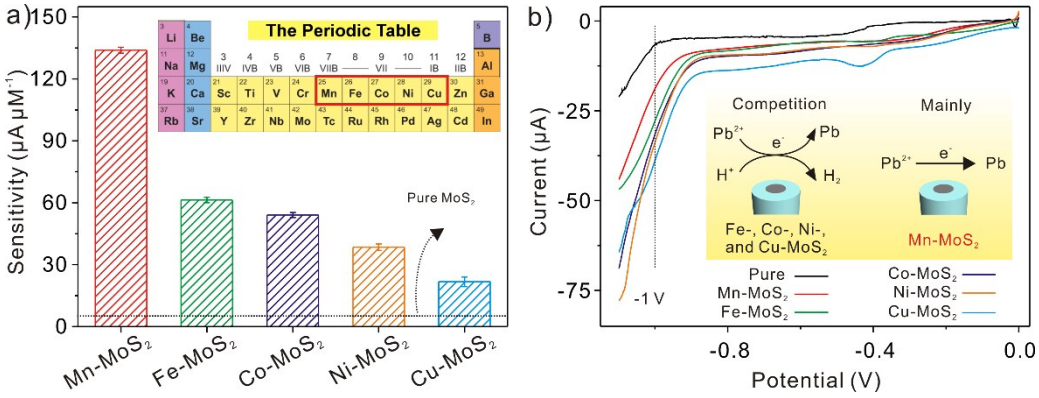

Fig. S15 Comparison of (a) electrochemical sensitivities and (b) hydrogen evolution capacity of pure and Mn, Fe, Co, Ni, and Cu-MoS_2. The inset of panel *a* and *b* is the periodic table and the effect of hydrogen evolution on electrochemical reduction

reaction, respectively.

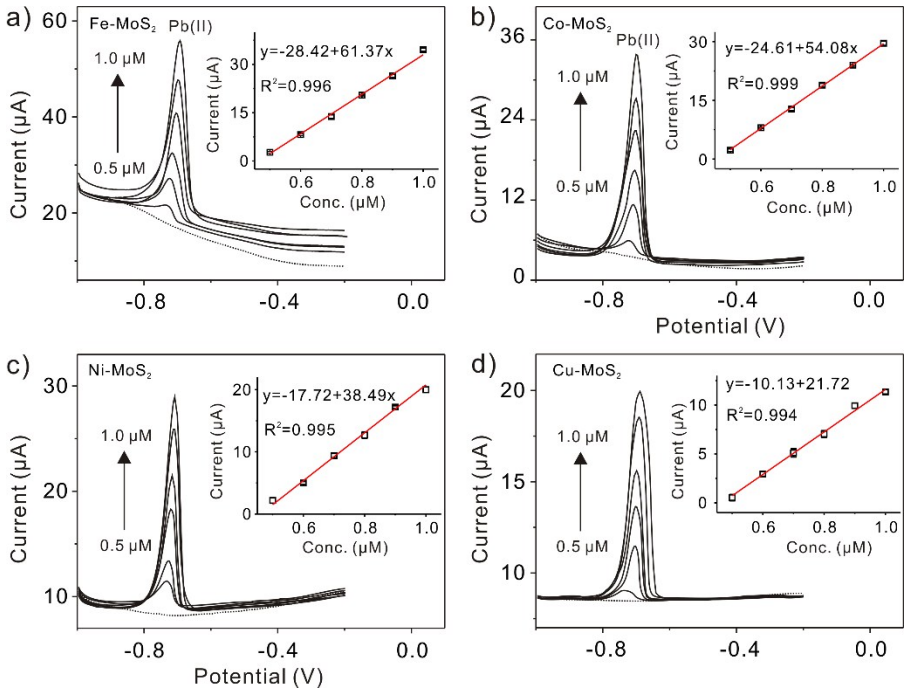

Fig. S16 Typical SWASV responses and corresponding linear calibration plots (insets) of (a) Fe-MoS_2, (b) Co-MoS_2, (c) Ni-MoS_2 and (d) Cu-MoS_2 modified GCE toward Pb(II). The error bars represent the standard deviations of five independent measurements of the same sample.

The stability and reproducibility are two important standards to assess the electrochemical detection performance. The relative standard deviation (RSD) of the 15 consecutive and repetitive responses to 0.3 μM Pb(II) at the Mn-MoS_2 is only 1.0% (Fig. S17a) demonstrating the good stability of this electrode. The reproducibility was assessed by measuring the response current after modifying ten GCE with Mn-MoS_2. The RSD of the current toward 0.1, 0.3, and 0.5 μM Pb(II) are 1.5%, 1.2%, and 1.3%, respectively (Fig. S17b), suggesting good reproducibility for Mn-MoS_2.

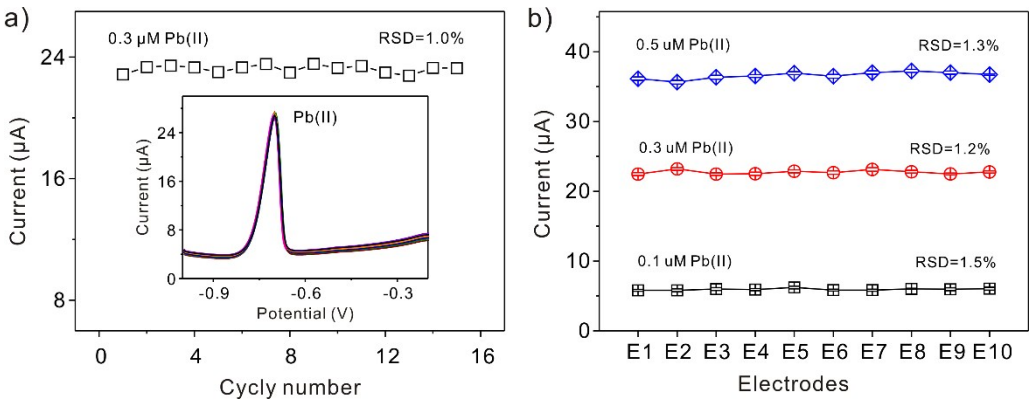

Fig. S17 (a) Stability measurement on Mn-MoS_2 modified GCE with repeated analysis of 0.3 μM Pb(II). (b) Reproducibility on the same GCE modified ten times repeatedly (No. E1-E10). All date are collected from every SWASV response in HAc-NaAc (pH 5.0) in spiked with 0.1, 0.3, and 0.5μM Pb(II). The error bars represent the standard deviations of five independent measurements of the same sample.

Table S1 Comparison on the electrochemical performance of different electrodes (noble metal, carbon, and metallic oxide) used for Pb(II) detection in the past three years.

Electrodes	Technique	Sensitivity ($\mu A\ \mu M^{-1}$)	Analysis time	Ref.
Au nanoparticles/GCE	DPASV	17.63	300 s	7
NiO/GCE	SWASV	13.46	120 s	8
Bi nanoparticle/GCE	SWASV	46.27	180 s	9
multi-walled carbon nanotubes/grapheme/GCE	DPASV	39.62	60 s	10
Bi/GCE	SWASV	48.73	200 s	11

Bi/Nafion/reduced graphene oxide-gold nanoparticle/GCE	SWASV	69.24	140 s	[12]
Glutathione/screen-printed carbon nanofiber electrode	SWASV	8.28	120 s	[13]
Mn-MoS_2/GCE	SWASV	133.90	120 s	This work

DPASV: differential pulse anodic stripping voltammetry.

Reference

1. L. Cai, J. He, Q. Liu, T. Yao, L. Chen, W. Yan, F. Hu, Y. Jiang, Y. Zhao, T. Hu, Z. Sun and S. Wei, *J. Am. Chem. Soc.*, 2015, **137**, 2622-2627.
2. Y. Shi, Y. Zhou, D.-R. Yang, W.-X. Xu, C. Wang, F.-B. Wang, J.-J. Xu, X.-H. Xia and H.-Y. Chen, *J. Am. Chem. Soc.*, 2017, **139**, 15479-15485.
3. L. Guo, H. Li and X. Gao, *J. Mater. Sci.*, 2004, **39**, 7041-7047.
4. Y. Sun, K. Liu, X. Hong, M. Chen, J. Kim, S. Shi, J. Wu, A. Zettl and F. Wang, *Nano Lett.*, 2014, **14**, 5329-5334; Q. Ding, F. Meng, C. R. English, M. Cabán-Acevedo, M. J. Shearer, D. Liang, A. S. Daniel, R. J. Hamers and S. Jin, *J. Am. Chem. Soc.*, 2014, **136**, 8504-8507.
5. K. Zhang, S. Feng, J. Wang, A. Azcatl, N. Lu, R. Addou, N. Wang, C. Zhou, J. Lerach, V. Bojan, M. J. Kim, L.-Q. Chen, R. M. Wallace, M. Terrones, J. Zhu and J. A. Robinson, *Nano Lett.*, 2015, **15**, 6586-6591.
6. G.-H. Hwang, W.-K. Han, J.-S. Park and S.-G. Kang, *Sens. Actuators, B*, 2008, **135**, 309-316.
7. X. Xu, G. Duan, Y. Li, G. Liu, J. Wang, H. Zhang, Z. Dai and W. Cai, *ACS Appl. Mater. Interfaces*, 2014, **6**, 65-71.
8. X. Li, H. Wen, Q. Fu, D. Peng, J. Yu, Q. Zhang and X. Huang, *Appl. Surf. Sci.*, 2016, **363**, 7-12.
9. C. Lin, W. Jie and J. Huangxian, *Chem.-Eur. J.*, 2015, **21**, 11525-11530.
10. H. Huang, T. Chen, X. Liu and H. Ma, *Anal. Chim. Acta*, 2014, **852**, 45-54.
11. H. Zhou, H. Hou, L. Dai, Y. Li, J. Zhu and L. Wang, *Chinese J. Chem. Eng.*, 2016, **24**, 410-414.
12. G. Zhao, H. Wang, G. Liu, Z. Q. Wang and J. Cheng, *Ionics*, 2017, **23**, 767-777.
13. C. Pérez-Ràfols, N. Serrano, J. M. Díaz-Cruz, C. Ariño and M. Esteban, *Talanta*, 2016, **155**, 8-13.